

Simulation of concrete fracture under different loading rates using rigid-body-spring networks

Kunhwi Kim & Yun Mook Lim

Yonsei University, Seoul, Korea

Sunyoung Choi

POSCO E&C Co.,Ltd., Hwaseong-si, Gyeonggi-do, Korea

John E. Bolander

University of California, Davis, California, USA

ABSTRACT: This paper presents the rate dependent fracture behaviors of concrete with different loading rates. The volume of concrete is discretized by an irregular lattice of rigid-body-spring elements, and the rate dependency is considered in the viscoplastic framework. The dynamic strength increase is obtained from the direct tensile test, and the viscoplastic properties are calibrated through comparisons with the experimental data. The flexural tests are performed with three-point-bending specimens under mixed-mode fracture and the effect of loading rate on the fracture pattern is achieved at slow and fast loading rates. The results of mixed-mode beam tests indicate that the fast loading could bring about the increase of strength and diagonal tension-shear failure contrast to flexural failure at the slow rate of loading. This study provides quantitative and qualitative understandings of the dynamic fracture under different loading rates

1 INTRODUCTION

Effects of dynamic loading on strength of materials have been reported in many experimental research results (Ross et al. 1989, Malvar & Ross 1999). Especially in concrete materials, the dynamic responses of materials are not only involved with strength but also accompanied with the cracking features (John & Shah 1990), which can be varied with different loading rates. Conventional numerical approaches have been adopted to simulate the dynamic increase of strength, but they have limitation to describe the cracking features during the fracture process. The distinct element method (DEM) and molecular dynamics (MD) can be instanced mostly as discrete model approaches where a material domain is considered as the assembly of elementary particles held together by interacting forces. As a macroscopic model, the former has been adopted to simulate the fracture process under highly dynamic loadings and grasp an interpretation of the characteristics (Masuya et al. 1994). Although this model has a respectable advantage to simulate the dynamic fracture over the usual frameworks of continuum mechanics, modeling with simple (spherical) particles gives difficulties to describe realistic material compositions. The latter, a microscopic and direct method of

analysis, has been recently attempted to understand the fundamental fracture mechanism (Wagner et al. 1992, Kim et al. 2008). The MD is based on basic rules in physics, and does not require experimentally precedent parameters. However, they should bear scale problems such as huge expenditure of computational resources for practical-size simulations.

In this study, the dynamic fracture behavior of concrete is simulated using rigid-body-spring network (RBSN) model (Bolander & Lim 2008). The material is modeled with the lattice of irregular cells interconnected by spring sets. Energy consuming mechanism is implemented in the elemental level during the fracture process (Bolander & Saito 1998, Berton & Bolander 2006), and the framework of Perzyna viscoplasticity is adopted in order to consider the rate dependency.

Numerical simulations are performed for the direct tensile test at various rates of loading. The strength increase effect is accomplished with the dynamic increase factor (DIF), the ratio of dynamic strength to the strength at static loading rate. The viscoplastic parameters are calibrated by comparing the DIFs with the results from the previous experimental research (Ross et al. 1989). Next, the rate effect on the failure mode is investigated through the location of crack paths in flexural beam test. The

specimen is under three-point-bend loading and a notch is offset from the midspan according to the fracture mode (mixed-mode). This paper discusses the numerical investigation of the effect of fast loading on the concrete fracture and gives a comprehensive description of failure mechanisms with different loading rates in meso-macroscopic frameworks.

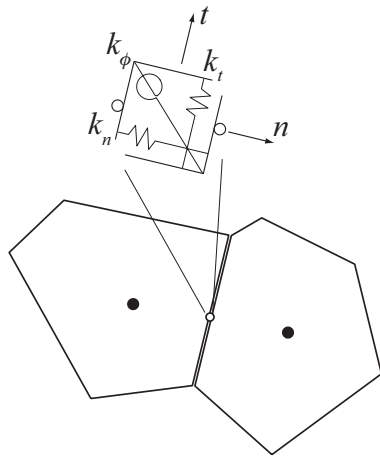


Figure 1. Spring set between two cells and the local coordinate.

2 NUMERICAL METHODOLOGY

2.1 Modeling of concrete fracture

The material is modeled by the RBSN, an assemblage of rigid cells interconnected along their facets with spring sets. The domain is discretized with the Delaunay-Voronoi dual tessellation to define the lattice topology. The spring set represents two translational and one rotational deformations in the local coordinate system $n-t-\phi$ as shown in Figure 1. The stiffness coefficients are calculated from the elastic properties of continuum and lattice geometries in a systematic manner.

Concrete fracture is described by imposing the damage variable to the stiffness of the spring according to the simple breaking rules. The constitutive relationship with tension softening is introduced to define the fracture process of the spring in n -direction of Figure 1. It is assumed that the compressive behavior is linearly elastic. For the tangential spring, the Mohr-Coulomb type failure criterion is applied to consider the fracture when the stress is over the yield surface. The yield surface is changed dependently as the normal spring is damaged. The damage variable is evaluated by the ratio of envelop stress on the criterion surface to the over-stress.

2.2 Time integration methods in dynamic problems

The kinematic trajectories of cells are computed by the explicit time integration schemes. In this study, Beeman's algorithm is used for calculating the dis-

placement and velocity vectors at every time step. However, at the initial step, the velocity Verlet algorithm is applied since the Beeman's algorithm needs the previous acceleration vectors during the integration. Both two algorithms are generally used in the MD simulations (Kim et al. 2008).

The verification of the accuracy of the numerical model is conducted through the simulation of 1-D elastic wave propagation problem. A bar in length of 1000 mm is discretized with 500 square cells as depicted in Figure 2a. The incident displacement wave is applied at the leftmost cell initially and the rightmost cell has a constraint to be fixed. The material properties are assigned as normal concrete; the elastic modulus $E=21.3$ GPa, and the density $\rho=2018$ kg/m³.

Figure 2b shows the longitudinal displacements of all cells at $t=0.2, 0.3, 0.35,$ and 0.5 ms. The direction of the reflected wave at the right boundary is reversed as a natural result. From the wave traveling distance versus the elapsed time, the wave velocity is estimated as 3246.7 m/s. This value is approximately agreed with the analytical wave velocity $\alpha=(E/\rho)^{0.5}=3248.8$ m/s.

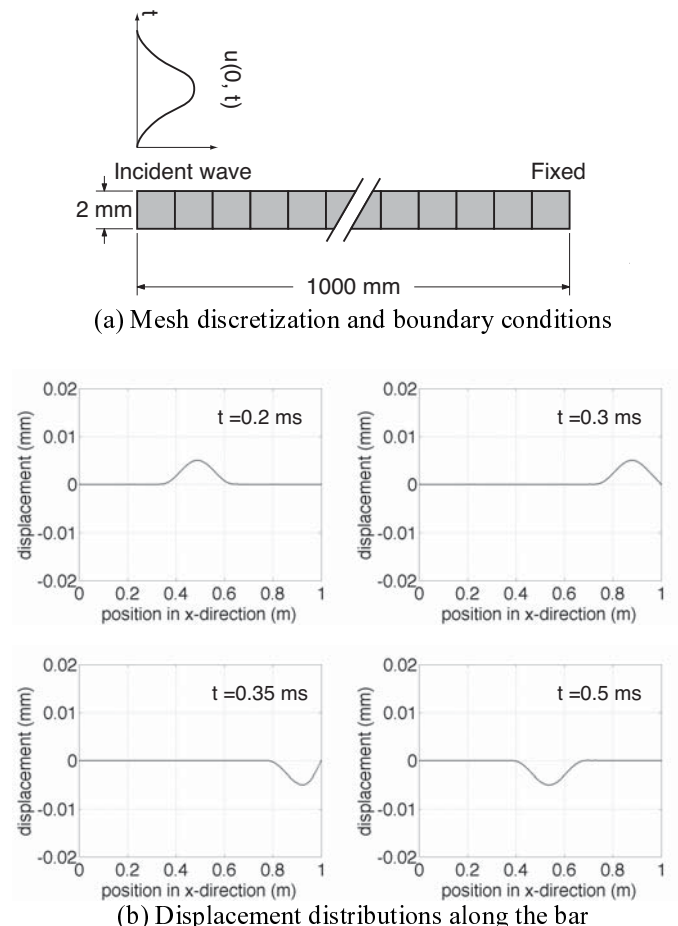


Figure 2. 1-D elastic wave propagation by an incident wave.

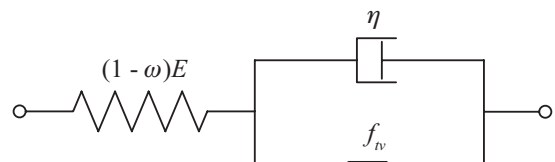


Figure 3. Rheological model with viscoplastic elements.

2.3 Viscoplasticity

Figure 3 depicts the schematic drawing of the rheological model. A spring for one degree of freedom has a connection in series with the viscoplastic elements. Here, the damage variable ω ($0 \leq \omega \leq 1$) is increased as the spring is fractured, and the stiffness of the spring is degraded by updating the damage variable. The viscoplastic strain contribution is described according to the Perzyna formulation. When the failure criterion is violated, i.e. when the yield function $f \geq 0$, the viscoplastic strain rate is expressed as

$$\dot{\epsilon}_{vp} = \frac{1}{\tau} \left(\frac{f(\sigma)}{f_v} \right)^N \frac{\partial f(\sigma)}{\partial \sigma} \quad (1)$$

where f_v represents the yield stress. The viscoplastic relaxation time is derived by $\tau = \eta/E$, and the fitting parameter $N \geq 1$, a real number.

The viscoplasticity describes the strength increase under dynamic loadings, which is associated to the micro-cracking process (Pedersen et al. 2008). Moreover, the retardation effect due to relaxation in the model could represent the change of fracture patterns as the loading rate varies. In section 3 and 4, the phenomena due to the rate dependency will be expressed through the simulations of the direct tensile tests and the flexural beam test.

3 DIRECT TENSILE TEST

The framework of the numerical analysis is applied to the simulation of the direct tensile test. The objective of the test is to evaluate the dynamic strength increase and calibrate the viscoplastic properties in Equation 1. A rectangular domain in dimensions of 100 mm by 50 mm is modeled with 140 cells. Figure 4 shows the discretized material specimen and the boundary conditions. The cells on the right boundary are loaded by force control while the leftmost cells are fixed. The loading rate is configured according to the simple elastic relationship for strain rate as $\dot{\epsilon} = \dot{\sigma}/E$ (Siregar et al. 2007). The stress is evaluated by measurement the reaction at the fixed boundary during the simulation, explicitly. The test is performed for 4 cases of strain rate, 10^{-2} , 10^0 , 10^1 , and 10^2 /s.

The increase of tensile strength is estimated with the DIF, the ratio of the measured strength to the static strength $f_i = 2.06$ MPa. The DIFs at the strain rates are plotted in Figure 5 and compared to the results from the previous experimental researches (Kormeling et al. 1980, McVay 1988, Mellinger & Birkimer 1966, Ross et al. 1989). Note that the tensile strengths of specimens and detailed ex-

perimental methods should be different—in the direct tensile tests and the splitting tensile tests, but the factors have similarity in their results. The numerical results have a good agreement with the experimental data.

By fitting the numerical results in the comparison of the DIFs, the viscoplastic properties are calibrated. The relaxation time τ is decided to be 5.5×10^{-7} s, and the fitting parameter $N = 1.5$. These parameters will be used in the next simulations.

Moreover, to consider the independency of spatial discretization, the direct tensile specimen is modeled by 880 cells and 3420 cells. The discretized specimens are simulated under the same conditions and 3 cases of the strain rate except for 10^{-2} /s are analysed. The DIFs of the simulations are also expressed in Figure 5, which are almost equal to the results of 140 cells; it is confirmed that the numerical framework is independent of the cell size. However, on the temporal aspect, the fine mesh discretization necessitates the short time step due to the numerical stability condition of the explicit time integration scheme.

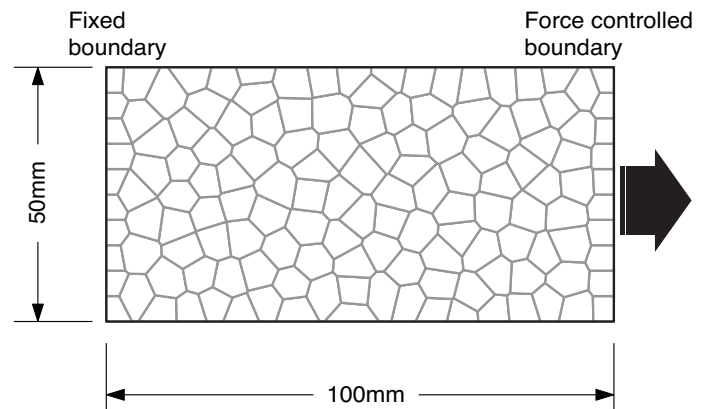


Figure 4. Configuration of the direct tensile test.

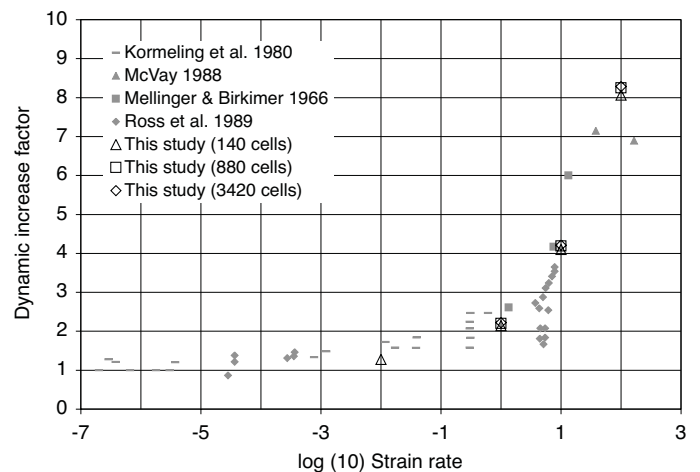


Figure 5. Dynamic increase factor of the tensile strength.

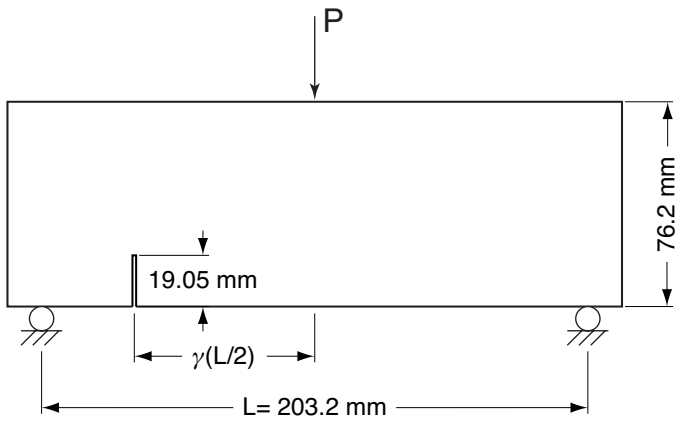


Figure 6. Dimension of the flexural beam test specimen and the boundary conditions.

4 FLEXURAL BEAM TEST

The qualitative analysis for strain rate effect on the failure mode is conducted in this section. Following the test program proposed by John & Shah (1990), the generic configurations of numerical experiment is shown in Figure 6. The flexural test is configured by the three-point-bending condition, and the fracture mode is controlled by offset of the notch along the span of the beam specimen. The location of the notch is defined by γ . The value of $\gamma=0.0$ indicates the mode I fracture configuration. A value of $\gamma \neq 0.0$ can result either in a mixed-mode failure at the notch tip or tension failure at the midspan, which is depending on the value of γ . With a specific value of γ , the failure can occur at both the notch tip and the midspan, called as the transition stage. The transition stage appears at different values of γ due to the loading rate in dynamic conditions; therefore, it is the rate dependent features in failure mode.

The applied velocity at the top are controlled according to the strain rate, 10^0 , 10^1 /s which is assessed at the bottom surface of midspan. For the location of the notch, 3 mixed-mode cases are considered, where the value of $\gamma=0.5$, 0.7, and 0.72, approximately. The material properties are retained as ones of the direct tensile test so that the calibrated viscoplastic parameters can be still applied.

Figures 7 and 8 show the comparison of crack patterns at the final failure state. The deformation is exaggerated by 5 times for visibility of cracks. Note that the bold-black-lined facets indicate the crack path although the crack is closed due to the main crack opening at the transition stage. For $\gamma=0.7$ in the figures, the transition stage occurs at the fast strain rate (Fig. 8b), whereas for the slow strain rate the failure only occurs at the midspan (Fig. 7b). John & Shah (1990) interpreted these failure features as

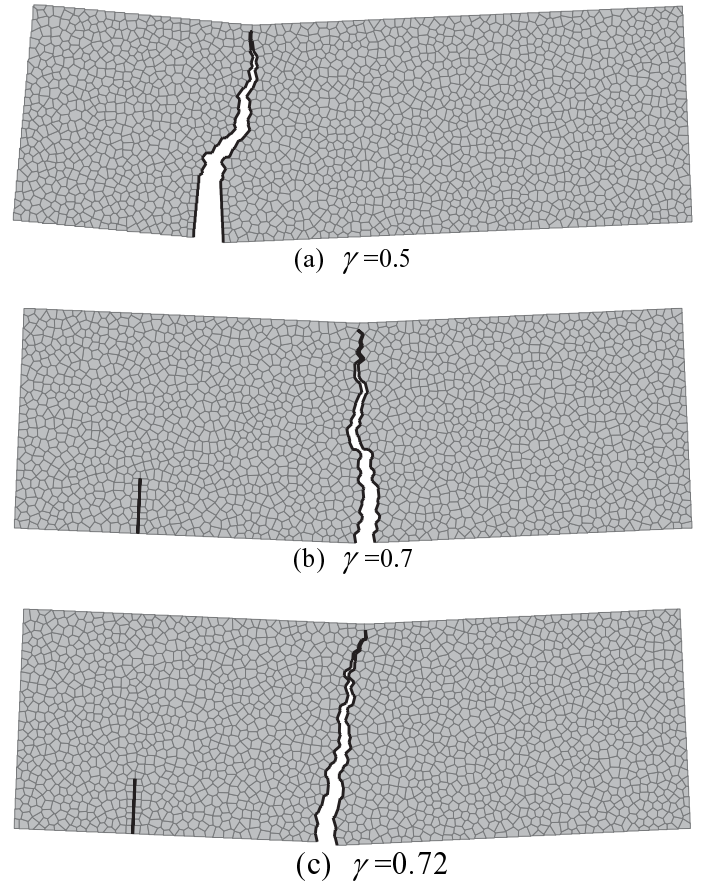


Figure 7. Mixed-mode failure paths at the slow strain rate.

that the failure in a ductile manner (flexural failure) at slow rates could turn into the failure in a brittle manner (diagonal tension-shear failure) at fast rates of loading. If we call the tendency to be failed at the notch tip in the mixed-mode as *notch sensitivity*, it can be interpreted that the notch sensitivity increases as the loading rate gets faster.

5 CONCLUDING REMARKS

The rate dependency of the concrete fracture is revealed through not only the increase of strength but also the change of failure patterns. This could be mainly due to the structural configurations whereas that is corresponding to the microscopic feature in the material. However, these characteristics should not be separated out to understand the rate dependent concrete fracture.

In this study, the rheological elements for the viscoplasticity are implemented in the RBSN model. The viscoplastic properties are calibrated through comparison with the previous experimental data. The numerical experiments are carried out to describe the rate effects under dynamic conditions. The remarks on the rate effects are arranged as follows:

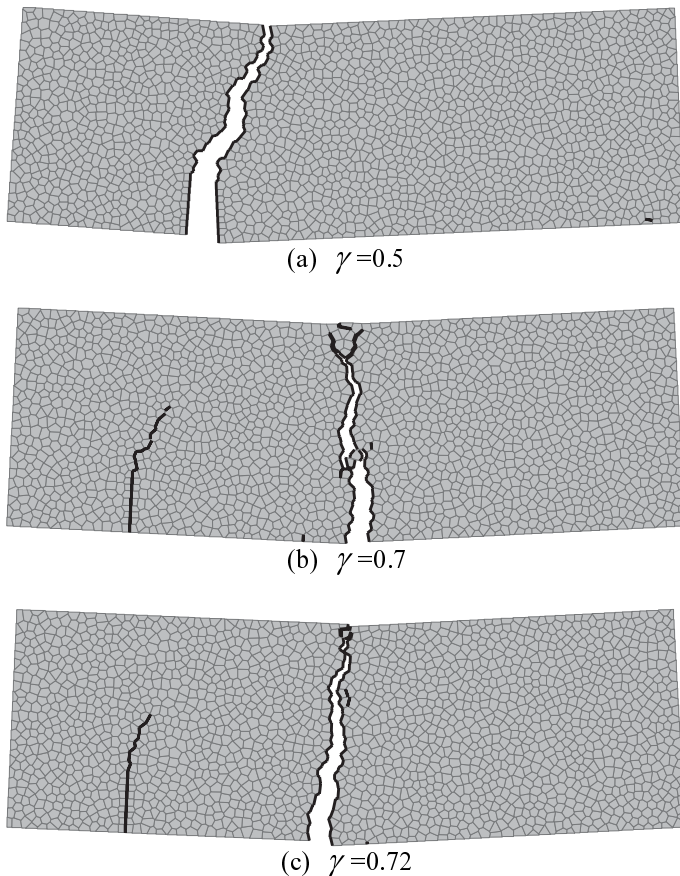


Figure 8. Mixed-mode failure paths at the fast strain rate.

- The direct tensile test is simulated under various loading rates, and the strength increase effect is observed with the increase of the strain rate.
- In the flexural test with notched beams, the transition stage appears at larger offset of the notch from midspan as the strain rate increases, i.e. the notch sensitivity grows at fast rate than slow rate of loading.

Although many researches on the rate dependent behavior of materials have been conducted in engineering fields, the limitation of facts is still existent. Extensive experiments and phenomenological data are furnished, but both quantitative and qualitative discussions are hardly mentioned. Besides, the experiments suffer from constraints in handling the equipments for controlling the dynamic behavior. The manners of setting loading conditions and measurement of loading rate might not be perfectly standardized yet. Thus, further considerations need to be focused on these subjects analytically as well as experimentally.

REFERENCES

- Berton, S. & Bolander, J.E. 2006. Crack band model of fracture in irregular lattices. *Computer Methods in Applied Mechanics and Engineering* 195: 7172-7181.
- Bolander, J.E. & Lim, Y.M. 2008. Simulation of fiber distribution effects in fiber-reinforced cement composites. In Paulino G.H. et al. (ed.), *Multiscale and Functionally Graded Materials 2006* 973:507-512. AIP Conference Proceedings.
- Bolander, J.E. & Saito, S. 1998. Fracture analyses using spring networks with random geometry. *Engineering Fracture Mechanics* 61: 569-591.
- John, R. & Shah, S. 1990. Mixed-mode fracture of concrete subjected to impact loading. *Journal of Structural Engineering* 116(3): 585-602.
- Kim, K., Lim, J., Kim, J. & Lim, Y.M. 2008. Simulation of material failure behavior under different loading rates using molecular dynamics. *Structural Engineering and Mechanics* 30(2): 177-190.
- Kormeling, H.A. et al. 1980. Experiments on concrete and single and repeated uniaxial impact tensile loads. In *Report No. 50-80-3*: 18-29. Stevin Lab., Delft Univ. of Tech.
- Malvar, L.J. & Ross, C.A. 1999. Review of strain rate effects for concrete in tension. *ACI Materials Journal* 95: 735-739.
- Masuya, H., Kajikawa, Y. & Nakata, Y. 1994. Application of the distinct element method to the analysis of the concrete members under impact. *Nuclear Engineering and Design* 150: 367-377.
- McVay, M.K. 1988. Spall damage of concrete structures. In *Technical Report No. SL-88-22*: 112-152. Vicksburg: U.S. Army Engineer Waterways Experiment Station.
- Mellinger, F.M. & Birkimer, D.L. 1966. Measurements of stress and strain on cylindrical test specimens of rock and concrete under impact loading. In *Technical Report No. 4-46*: 71. Cincinnati : U.S. Army Corps of Engineers, Ohio River Division Laboratories.
- Pedersen, R.R., Simone, A. & Sluys, L.J. 2008. An analysis of dynamic fracture in concrete with continuum visco-elastic visco-plastic damage model. *Engineering Fracture Mechanics* 75: 3782-3805.
- Ross, C.A., Thompson, P.Y. & Tedesco, J.W. 1989. Split-hopkinson pressure-bar tests on concrete and mortar in tension and compression. *ACI Materials Journal* 86(5): 475-481.
- Siregar, R.A., Daimaruya, M. & Fuad, K. 2007. Dynamic splitting-tensile test and numerical analysis for brittle materials. In Senin, H.B. & Idris N.H. (ed.), *Proceedings of Solid State Science and Technology, ICSSST 2006* 909: 68-73. AIP Conference Proceedings.
- Wagner, N.J., Holian, B.L. & Voter, A.F. 1992. Molecular-dynamics simulation of two-dimensional materials at high strain rates. *Physical Review A* 45(12): 8457-8470.